FLSEVIER

Contents lists available at ScienceDirect

Engineering Fracture Mechanics

journal homepage: www.elsevier.com/locate/engfracmech



Overcoming the convergence difficulty of cohesive zone models through a Newton-Raphson modification technique



Reza Sepasdar, Maryam Shakiba*

Department of Civil and Environmental Engineering, Virginia Tech, 750 Drillfield Dr., Blacksburg, VA 24061, USA

ARTICLE INFO

Keywords:
Cohesive zone
Convergence difficulty
Finite element
Numerical instability
Interface debonding

ABSTRACT

This paper studies the convergence difficulty of cohesive zone models in static analysis. It is shown that an inappropriate starting point of iterations in the Newton–Raphson method is responsible for the convergence difficulty. A simple, innovative approach is then proposed to overcome the convergence issue. The technique is robust, simple to implement in a finite element framework, does not compromise the accuracy of analysis, and provides fast convergence. The paper explains the implementation algorithm in detail and presents five application examples. It is concluded that the method is computationally efficient, has a general application, and outperforms the existing methods.

1. Introduction

Cohesive zone models (CZMs) are popular methods to simulate fracture in engineering applications. Delamination of layered composites, crack propagation in materials, and debonding of fiber/matrix interfaces in fiber-reinforced composites are examples of CZMs applications [1–6]. The cohesive models are easy to implement within a finite element (FE) framework and adaptable to other nonlinear constitutive models. CZMs were utilized in extended finite element method (XFEM), which enable modeling arbitrary crack propagation within materials [7–9]. Generally, CZMs were proven to be efficient, robust, and more accurate compared to continuum damage and fracture mechanics theories [10–13]. However, cohesive models can encounter convergence difficulty in a static analysis once failure initiates [14–18]. The convergence issue reduces CZMs efficiency and limits their range of applications.

Researchers studied the root of the convergence difficulty in CZMs and categorized it into two main groups of physical and numerical instability [10,19,11,20,13]. Several studies explained that fracture initiation and propagation is intrinsically a dynamic phenomenon. Thus, physical instability due to the lack of kinetic energy and inertial forces in static analysis causes the convergence issue [21,22,19,20,23]. Other studies, however, conjectured that numerical instability due to either a solution jump after failure or the presence of multiple solutions is responsible for the convergence difficulty [10,13]. Several methods were consequently developed to resolve the convergence difficulty based on the hypothesized root of the issue.

The most common existing methods to overcome the convergence difficulty in CZMs are viscous regularization [10,19], decrease of global displacement (known as Riks method) [24], and full dynamic analysis [21,22]. The different points of view on the convergence difficulty of CZMs and their performances for static frameworks are explained in detail in Section 2.1. In summary, the available methods to overcome the convergence difficulty in static analysis make the computations expensive, compromise the accuracy, or require complex programming. Likewise, full dynamic analysis (implicit or explicit) is computationally very costly. Therefore, it is imperative to revisit and fully understand the root of the convergence difficulty and propose a method to resolve this

E-mail address: mshakiba@vt.edu (M. Shakiba).

^{*} Corresponding author.

issue efficiently.

In this paper, the behavior of CZMs under static loading and their convergence issue in an FE analysis are comprehensively studied through one-dimensional (1-D) and two-dimensional (2-D) representative examples. The Newton–Raphson (NR) iteration at the moment of instability based on a new point of view is analyzed. The NR analysis sheds light on the actual root of the convergence difficulty. A novel and simple method for overcoming the convergence issue is then presented and proven to be efficient and robust. All concepts presented in this research, as well as the proposed method, can easily be generalized to three-dimensional (3-D) analyses.

This paper is organized as follows. The behavior of cohesive interfaces, their implementation within an FE framework, different points of view on the convergence difficulty, and the existing solutions in the literature are discussed in Section 2. The actual root of the convergence difficulty is then determined based on the examination of the NR iterations at the moment of instability in Section 3. Subsequently, a novel method is proposed in Section 4 to overcome the convergence issue. In the end, five application examples are presented to demonstrate the validity, robustness, and efficiency of the proposed method.

2. Cohesive zone model behavior

Several CZMs were developed in the literature to express the interface behavior based on application problems. The models use nonlinear functions, including exponential [25–27], bilinear [28–30], trapezoidal [31,32], parabolic [33,34]. Various functions may have different performances and convergence rates depending on the mesh size, geometry, and material properties in an FE simulation [14,35]; however, their general behavior is similar. Thus, an exponential function as a typical traction-separation or debonding law is adopted in this work to study the behavior of CZMs. The exponential function was chosen as it merely provides a better visual presentation of the idea in this work. In the exponential model [26], the traction in the interface, σ , is related to the effective opening displacement, δ , by

$$\sigma = \frac{\sigma_c}{\delta_c} \delta e^{(1-\delta/\delta_c)} \tag{1}$$

where σ_c is the cohesive strength of the interface corresponding to a critical opening displacement δ_c . This exponential CZM is schematically presented in Fig. 1 (a).

A few models are available in the literature to calculate CZMs' effective opening displacement in the case of mixed-mode loading,

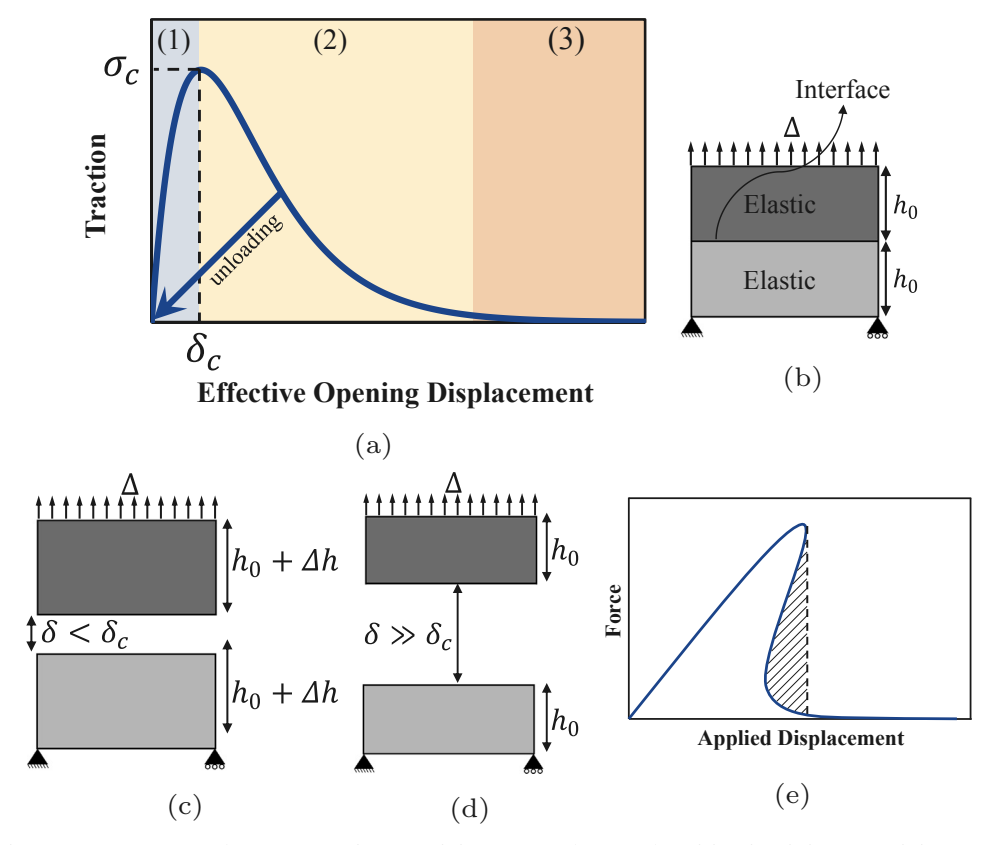


Fig. 1. (a) A schematic representation of an exponential CZM and three stages of an interface debonding behavior, and (b), (c), (d) demonstrate debonding stages of a simple elastic bar with an interface, and (e) a schematic representation of a snap-back resulting from the decrease of applied displacement.

which account for the interaction between normal and tangential behavior of interfaces [36,32,26,37]. In this paper, the coupling between the normal and tangential debonding is defined based on a proposed relation by Ortiz and Pandolfi [26]

$$\delta = \sqrt{\delta_n^2 + \beta \delta_t^2} \tag{2}$$

where β is a factor between 0 and 1 that differentiates between the normal and tangential interface debonding. If $\beta = 1$, δ becomes the true distance between the pair nodes of the interfaces.

The CZM is presented in 1-D in this section but can be easily extended to 3-D cases. It must be noted that the concepts and methods presented in this paper have a general functionality and are independent of the types of CZMs' behavior.

2.1. Convergence difficulty

To study the behavior of cohesive interfaces, a simple elastic bar with an interface in between, as illustrated in Fig. 1 (b), is considered. The elastic bar is restrained at the bottom while a static monotonic displacement, Δ , is applied at its top boundary. The applied displacement on this bar is equal to the induced opening displacement in the interface, δ , in addition to the deformation in the elastic bar, $2\Delta h$. By applying the displacement on the elastic bar, the interface starts to debond while its traction increases. Fig. 1 (c) schematically illustrates this debonding initiation stage, which corresponds to phase one in Fig. 1 (a). Once the interface fails (i.e., $\delta > \delta_c$), the interface traction decreases while its opening displacement increases. In this stage, elastic deformation in the bar recovers, which is related to phase two in Fig. 1 (a). By increasing the applied displacement, the interface traction decreases until it converges to zero, which corresponds to phase three in Fig. 1 (a). The elastic parts, then, completely recover to their initial undeformed shape. Any further increase in the applied displacement is followed by a rigid body movement of the top elastic part, as it can be seen in Fig. 1 (d).

It is known that if the elastic material's stiffness is low compared to the interface's local tangent stiffness, the failure happens instantaneously and causes instability in the numerical solution [10]. An instantaneous failure of the interface implies that the interface traction quickly drops to zero, which is followed by a sudden deformation recovery in the elastic parts. This phenomenon is known as a solution jump, which causes convergence difficulty in static analyses [13,10]. Several researchers explained the sudden recovery as a dynamic phenomenon and represented it by a snap-back in the total force—displacement response as it is schematically shown in Fig. 1 (e) [13,19,23,20]. The snap-back portion results from the decrease in the applied displacement, and its area is argued to be equal to the missing kinetic energy in static analyses. After the snap-back portion is passed, the applied displacement can be increased again, and the convergence is easy afterward. Based on different reasoning on the roots of the convergence difficulty, several methods were proposed to resolve this issue. The most common methods are explained in the next subsection.

2.2. Existing Methods for Overcoming the Convergence Difficulty

One possible solution to address the convergence difficulty in CZMs is to decrease the applied displacement. This solution typically uses the arc-length (Riks) iterative method due to its path-finding feature [24,38]. The arc-length method does not compromise the accuracy, and it is robust in addressing the convergence difficulty for the CZM functions without a sharp turning point [11,18,13]. However, if there is a sharp turning point in the CZM function (e.g., the bilinear model), the arc-length method fails to overcome the convergence difficulty [18,13]. Moreover, the programming of the arc-length method is not as simple as the NR method. The method requires additional displacement steps to capture the snap-back portion as well as additional constraint equations to be solved in each iteration. [39]. Hence, the arc-length method is relatively computationally expensive.

Another common method to resolve CZMs' convergence difficulty is the well-known viscous regularization method [10,19]. The viscous regularization method adds a so-called artificial viscosity term to the cohesive zone constitutive behavior to facilitate the convergence. The proponents of the physical instability as being the root of convergence difficulty argue that the artificial viscosity compensates for the missing kinetic energy in static analyses. Chaboche et al., [10] and Yu et al., [13], however, believed that the artificial viscosity would fix a numerical instability, which prevents the convergence of NR iterations. Viscous regularization approach has gained more popularity compared to other methods due to the ease of implementation and its high convergence rate. The method, however, requires altering the cohesive constitutive behavior, which necessitates a sensitivity analysis on the effect of the artificial viscosity coefficient. It also requires additional displacement steps to simulate the instantaneous failure of the interface.

Other methods that use damage in contacts and interfaces based on continuous/discontinuous Galerkin formulation are available in the literature [40–43]. The methods do not depend on node-to-node springs, have acceptable performance when the meshes are non-conforming, and are capable of modeling tension debonding, compression damage, and frictional sliding. These specially formulated contact elements are robust in handling instabilities and have high convergence rates. There are a few other proposed methods for addressing CZMs' convergence issue in the literature that are less popular due to their inefficiency and complexity. These methods are briefly reviewed here. One proposed approach is to reduce the mesh size as it decreases the convergence difficulty due to local instabilities [44,10]. However, excessive mesh refinement decreases the efficiency of numerical analysis. Another alternative is to use quasi-Newton iterative methods, which do not have a quadratic convergence and are thus slow. Additional treatments were proposed to accelerate the convergence speed of quasi-Newton iterative methods [23]. Recently, Gu et al., [20] proposed the inclusion of inertial forces in the CZMs' constitutive behavior instead of artificial viscosity to compensate for the lack of kinetic energy. This method requires special programming, which involves solving a system of nonlinear equations for the increments with the convergence issue. There are also a few other methods in the literature to resolve the CZMs' convergence issue based on continuum

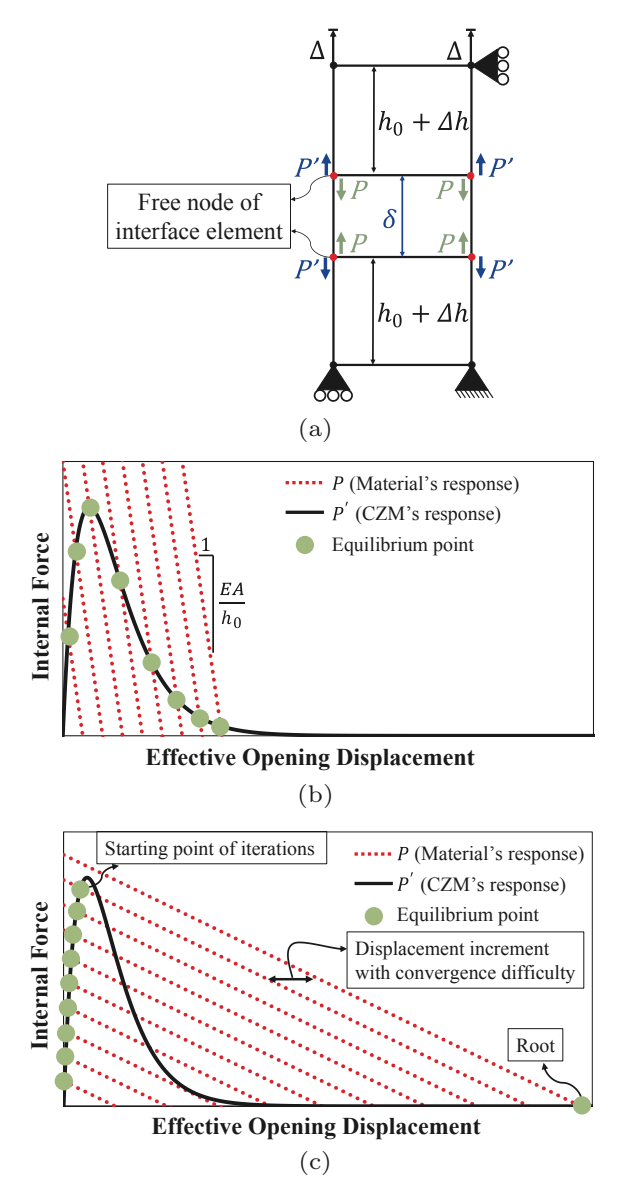


Fig. 2. (a) A simple model with a horizontal interface between two elastic materials, and (b) and (c) represents the simple model responses for the cases when the material stiffness (i.e., EA/h_0) is close to the CZM's local tangent stiffness, and when the material stiffness is less than the CZM's local tangent stiffness, respectively. The dots represent equilibrium points, which are the intersection of the elastic material and CZM responses, under monotonically increasing applied displacement.

damage mechanics [45,46].

In summary, the existent methods in the literature have limited applications due to their complexity, implementation difficulties, and increase in the computational costs [10]. Therefore, it is necessary to comprehensively analyze the convergence difficulty related to CZMs and propose an efficient method to resolve this issue.

3. Analysis of CZMs' convergence difficulty

In this section, the convergence difficulty of CZMs in static frameworks is studied through monitoring NR iterations at the moment of instability. It must be pointed out that the CZM, simple representative FE model, and discussions presented in this section are in a 2-D framework, but can easily be extended to 3-D analyses.

To demonstrate the simulation of FE models with cohesive interfaces under static displacement controlled conditions, a simple model, as presented in Fig. 2 (a), is considered. The FE model consists of two identical elastic 4-node elements with a modulus of elasticity E that are connected via a cohesive interface. The elastic elements have a length of h_0 , and a cross-sectional area of A. The displacement, Δ , is applied to the top of the model and is increased monotonically. The goal is to calculate the vertical displacement

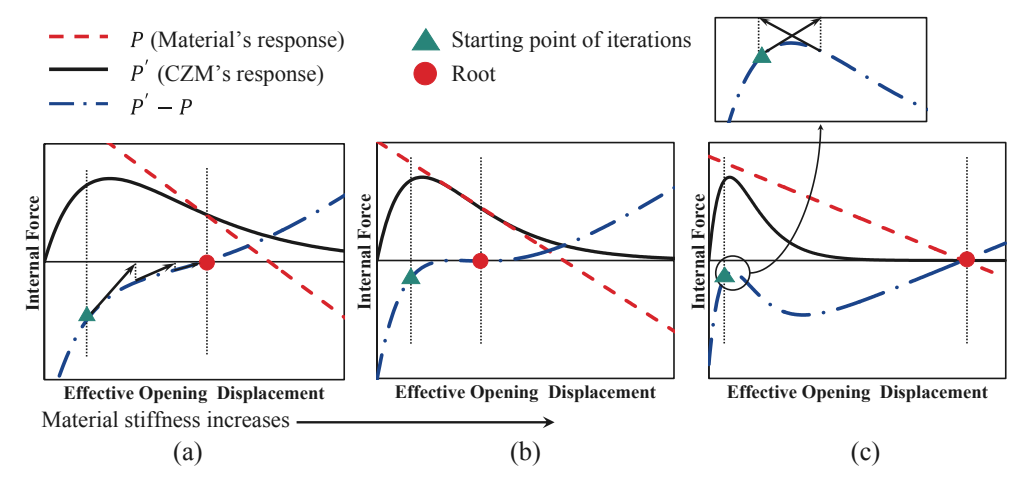


Fig. 3. The solutions of the simple elastic bar model at the cohesive zone failure step for the cases of (a) an easy convergence, (b) the threshold between an easy and a difficult convergence, and (c) a difficult convergence.

of the free nodes such that equilibrium is satisfied. Each free node of the interface element is shared by an adjacent elastic element, as shown in Fig. 2 (a). For equilibrium to be maintained throughout the analysis, the sum of the internal forces at each interfacial node must be equal to zero. The internal forces include the forces applied by the material (P') and the CZM (P). Therefore, at each displacement increment, P' - P = 0 must hold.

Fig. 2 (b) and (c) illustrate the solution to the described example. The P' function represents the CZM's response, while the P functions are material's responses to the applied displacement. The horizontal distances between the P functions are equal to the applied displacement increments, and CZM's responses intersect. The equilibrium points shown in Fig. 2 (b) and (c), need to be computed at each displacement increment using the NR method. It is evident in Fig. 2 (b) that when the material stiffness (i.e., EA/h_0) is larger than the CZM's local tangent stiffness, the equilibrium points are close to one another. Hence, the convergence is easy and fast throughout the analysis. However, when the material stiffness is less than the CZM's local tangent stiffness, the solution jump occurs at the CZM's failure increment, as seen in Fig. 2 (c). As a consequence, the starting point of iterations in the NR method and the root are far apart, and the convergence is difficult.

It is worthwhile to study the NR iterations at the CZM's failure increment more closely to examine the effects of the solution jump and the relative stiffness. The NR step to solving for P'-P=0 at the failing of cohesive zone increment is illustrated in Fig. 3 for three different material stiffnesses. It must be noted that the previous converged solution is always somewhere around CZM's failure point. The P'-P function is the subtraction of material and CZM responses. Hence, the root is where this function intersects with the horizontal axis. The different cases presented in Fig. 3 are as follows:

- (a) The material is stiff relative to the CZM's local tangent stiffness. Therefore, the P'-P has a well-behaved ascending function, and the NR iterations converge to its root with no difficulty, as it is schematically illustrated in Fig. 3 (a).
- (b) The material's stiffness is equal to the CZM's local tangent stiffness. Hence, the resulting P' P function has an inflection point where it intersects with the horizontal axis, as shown in Fig. 3 (b). This case forms a threshold between an easy and a difficult convergence.
- (c) The material is soft relative to the CZM's local tangent stiffness. In this case, P' P function has a local maximum close to the starting point of iterations, which is the last converged solution, as it is schematically shown in Fig. 3 (c). As a consequence, there is a chance that the NR iterations enter an infinite cycle of iterations and do not converge.

Therefore, it can be seen that in static analyses, numerical instability is the root of the CZMs' convergence difficulty. In light of this knowledge, the performance of the two most popular methods described in Section 2.2 (i.e., viscous regularization and decrease of global displacement) can be studied in more detail.

3.1. Evaluation of the two common methods to resolve the convergence difficulty: Viscous regularization, and decrease of global displacement methods

In the viscous regularization method, the inclusion of a rate-dependent term in the cohesive function causes a decrease in the post-failure decay rate. This treatment, in turn, regularizes the local maximum of the P'-P function in Fig. 3 (c) and forces it towards an inflection point with a horizontal slope similar to the case in Fig. 3 (b). The regularization facilitates the convergence. However, as a consequence, an instantaneous failure is simulated as being slow and non-instantaneous, which may significantly affect the stress distribution within the FE analysis. Therefore, a smaller viscosity coefficient needs to be used to ensure that the viscosity is not negatively affecting the stress distribution. A smaller viscosity coefficient leads to several time step refinements.

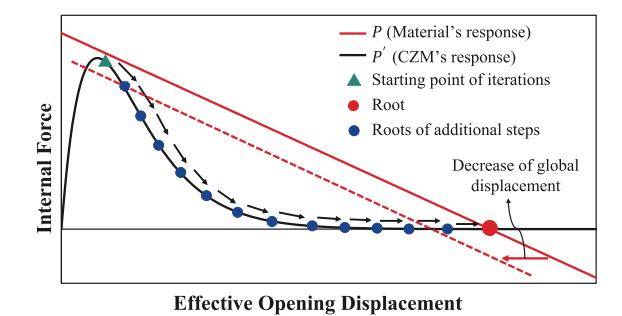


Fig. 4. The path to be traveled towards convergence via extra displacement increments in the decrease of global displacement method.

In the decrease of global displacement method, the applied displacement is decreased after the convergence difficulty is encountered. As a result, the convergence is towards the roots on the decaying portion of the CZM through additional equilibrium points, as illustrated in Fig. 4. As can be seen, the convergence is ultimately towards the root that could not converge in the first place. The decrease of global displacement method converges to the accurate root eventually and can simulate an instantaneous failure. However, the method is not simple to implement and is computationally expensive.

4. Proposed novel method to resolve CZMs' convergence difficulty

The previous section described that an inappropriate starting point of iterations, located in the vicinity of a local maximum, is responsible for the convergence difficulty of CZMs. This section presents a method for addressing the convergence issue. The proposed procedure is based on modifying the starting point of the problematic NR step at the failure increment. The modification is applied only to the pair nodes of the interface elements (PNIEs), causing the convergence problem. The term "starting point of iterations" in this context refers to the effective opening displacement of PNIEs at the previous converged step.

Fig. 5 (a) illustrates the solution to the simple model presented in Fig. 2 (a) at the interface's failure increment for a case with

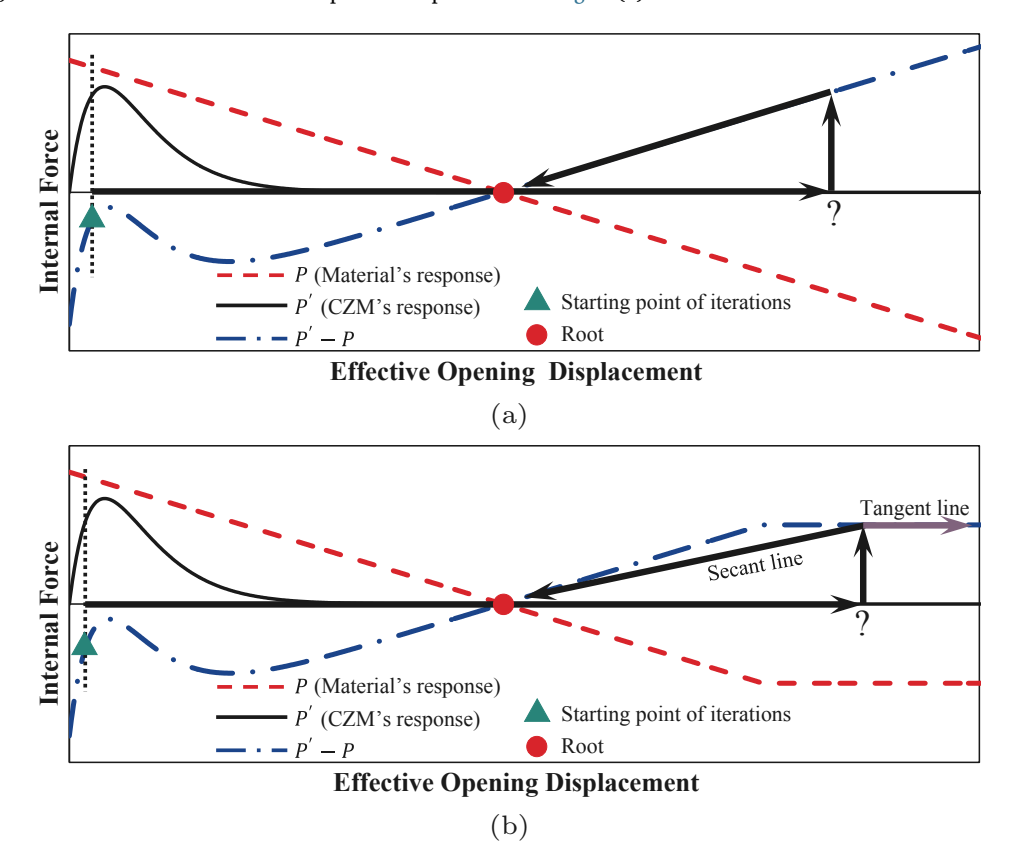


Fig. 5. Modification of the starting point of iterations for the case of (a) elastic material, and (b) nonlinear material behavior, which can be defined by either tangent stiffness or secant stiffness.

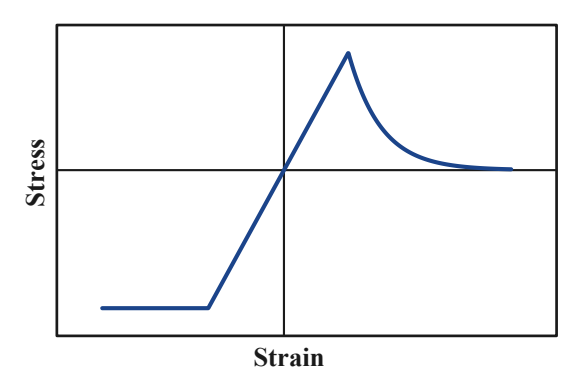


Fig. 6. An example of a nonlinear behavior for a brittle material.

convergence difficulty. It is noted that if the starting point of iterations locates anywhere on the right linear ascending portion of the P'-P function, the NR iterations quickly converge to the root. Hence, the displacement of the problematic PNIE can be modified such that the starting point of iterations occurs on the linear ascending portion of the P'-P function. For a linear elastic material behavior, any starting point on the linear ascending part leads to fast and easy convergence.

For the case of materials with nonlinear behavior, a constitutive law as presented in Fig. 6 is assumed as a typical example. The material is brittle under tension and elastic-perfectly-plastic under compression. For the simple model presented by Fig. 2 (a), any enforced debonding along the debonding direction subjects the material to pure compression. As a result, the rightmost portion of the P function, as illustrated in Fig. 5 (b), becomes horizontal following the material's behavior under compression (i.e., elastic-perfectly-plastic). The leftmost portion of the P' - P function follows the material's behavior under tension, which is not included in the plot as it does not affect the proposed method. When the modification is applied to the starting point of iterations, it may end up on the horizontal portion of P' - P function, as illustrated in Fig. 5 (b). Once the starting point locates on the horizontal part, the performance of the proposed method in addressing the convergence issue depends on how the material's stiffness matrix is defined in an FE framework.

If the material's behavior is defined using the material's tangent stiffness matrix, once increasing the starting point of iterations, the NR diverges from the root following the tangent slope of the P'-P function. In FE simulations, however, the secant stiffness matrix is typically used to define a nonlinear material behavior, particularly when damage models represent the nonlinearity. Fig. 5 (b) illustrates that if the secant stiffness matrix defines the material's constitutive behavior, increasing the starting point of iterations causes the iterations to quickly converge to the root following the secant slopes of the material's response. Hence, the starting point can be increased by any large magnitude to ensure that it locates beyond the problematic local maximum of the P'-P function, and the convergence is guaranteed. It should be noted that the use of the secant stiffness matrix, in general, causes a superlinear convergence rate. Hence, the overall convergence rate is slower than quadratic but faster than linear convergence rates.

When the secant stiffness is used to define the material's behavior, whereas the tangent stiffness defines the CZM's response, the following features can be mentioned regarding the global stiffness matrix:

- (a) At the initial nonlinear portion of the P' P function in Fig. 5 (b), the iterations follow a path defined by the tangents of the P' P function since the CZM's nonlinear behavior is determined by tangent stiffness (i.e., the P' function).
- (b) At the central linear ascending portion of the P'-P function where the contribution of CZM's behavior is diminished, the tangent and secant stiffness matrices are the same.
- (c) At the end horizontal portion of the P' P function, the iterations follow a path defined by the material's secant stiffness.

The effect of the material's tensile behavior on the application of the proposed method is important to study. Depending on the material's tensile strength, either of the two scenarios can happen:

- (a) If the material's tensile strength is smaller than the CZM's cohesive strength, the material fails before the interface, and the opening displacement of the interface recovers. Since the interface does not fail in such cases, there is no convergence issue resulting from the CZM.
- (b) If the material's tensile strength is greater than the CZM's cohesive strength, the interface fails, and the bulk material has elastic deformation recovery. Hence, the CZM might cause convergence difficulty. In this case, if the material is brittle with a steep post-failure decay in tension, there may be three equilibrium roots at the failure increment, as it is depicted in Fig. 7. The correct root is the one that corresponds to the failure of the interface, followed by a deformation recovery in the material (the rightmost root). Since the modification increases the abscissa of the starting point of iterations, the convergence is still towards the rightmost root in Fig. 7. As a result, the presence of the other two roots has no influence on the performance of the proposed method.

Thus far, the performance of the proposed method was studied on a simple model. In general, interfaces may undergo mixed-modes of debonding in models with complex geometries. Hence, the application of the proposed modification to a PNIE causes a

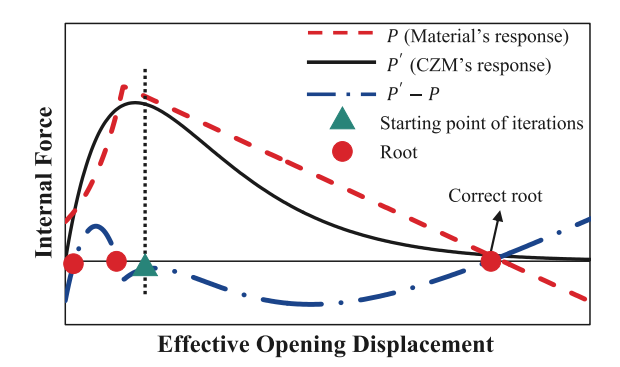


Fig. 7. Presence of multiple roots for the step with convergence difficulty if the material is brittle under tension with a steep post-failure decay.

general state of stress to be induced within the adjacent material. Under this condition, the response of the material (i.e., the shape of the *P* function in Fig. 5 (b)) is tough to predict. However, as long as the secant stiffness defines the material's constitutive behavior, the proposed method does not depend on the shape of the material's response. Therefore, the presented discussions can be generalized to any arbitrary mode of debonding. Hence, any problematic PNIE can be simply modified as described in this section once they are detected in the FE model. The algorithm for detecting and modifying the problematic PNIEs are explained in detail in the following subsections.

4.1. Detecting the problematic PNIEs

The process of detecting problematic PNIEs for the case of CZMs with the exponential behavior as presented in Eq. (1) is explained in this section. It should be noted that in the derivations in this section, the material behavior is assumed as linearly elastic before failure. Detecting the problematic PNIEs for other materials and CZMs constitutive equations can be achieved following the same procedure.

As it was explained in the previous section, the oscillation during the infinite cycle occurs about the local maximum of the P'-P function, as it can be seen in Fig. 3 (c). Hence, one way of detecting the problematic PNIEs is to calculate the abscissa of the P'-P function's local maximum for all PNIEs in the FE model. The next step is to check if the effective opening displacement of the PNIE is oscillating about the local maximum point. This process, however, requires the knowledge of the material's stiffness (i.e., slope of the P' function in Fig. 3 (c)) corresponding to all PNIEs throughout the FE model, which is costly to compute. An easier and more efficient way of detecting the problematic PNIEs can be achieved. It can be shown that the starting point of iterations corresponding to a problematic PNIE, always occurs within an interval.

The lower bound of the interval can be calculated by realizing the fact that the starting point of iterations for the problematic PNIEs is always greater than δ_c . This is schematically illustrated in Fig. 8, which depicts the converged solution of the previous step (i.e., the starting point of iterations for the current step). As a result, the lower bound of the interval is equal to δ_c .

The upper bound of the interval corresponds to the threshold case between an easy and a difficult convergence, as it can be seen in Fig. 3 (b). In this case, neglecting the Poisson's ratio effect, P and P' can be defined as follows:

$$P' = \frac{\sigma_{\rm c}}{\delta_{\rm c}} \delta \ e^{(1-\delta/\delta_{\rm c})} \left(\frac{A}{2}\right) \tag{3}$$

$$P = B_1 \delta - B_0 \tag{4}$$

where B_1 and B_0 are two unknowns. A/2 indicates that half of the load in the interface is carried by each PNIE. The P'-P in the vicinity of the root for the previous converged step is

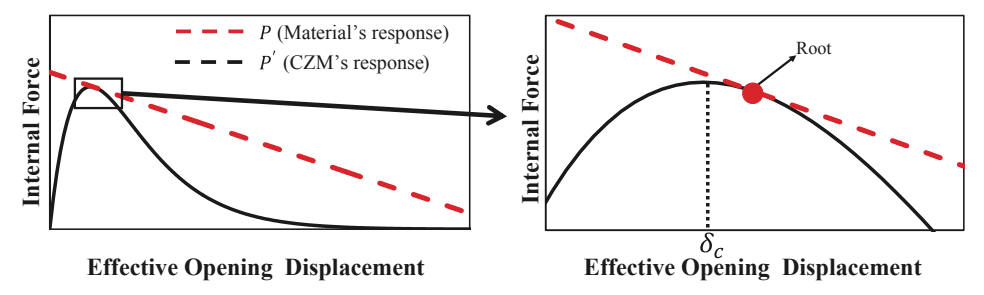


Fig. 8. Location of starting point of iterations for the step with convergence difficulty.

$$P' - P = \frac{\sigma_c}{\delta_c} \delta e^{(1 - \delta/\delta_c)} \left(\frac{A}{2}\right) - (B_1 \delta - B_0) \tag{5}$$

The root in the threshold case is the abscissa of the inflection point, which can be calculated by taking the second derivative of Eq. (5) and setting it equal to zero, which is

$$\frac{d^2(P'-P)}{d\delta^2} = \sigma_c e^{(1-\delta/\delta_c)} \left(\frac{A}{2}\right) \left(\frac{-2}{\delta_c^2} + \frac{\delta}{\delta_c^3}\right) = 0 \tag{6}$$

By solving the above equation, the interval's upper bound is calculated to be $\delta = 2\delta_c$.

Hence, the effective opening displacements of the problematic PNIEs at the beginning of the iterations for the step with convergence difficulty always occurs somewhere between δ_c and $2\delta_c$. It must be noted that the calculated interval is typically very short as δ_c is normally chosen to be a very small number to ensure strain continuity before the failure of the interface. However, there is still a small chance that the effective opening displacement of a non-problematic PNIE occurs within the interval at the moment of instability. In this case, the P'-P is a monotonically increasing function with only one root, as illustrated in Fig. 3 (a), and hence, any starting point of iterations has an easy convergence. Therefore, applying the modification to a non-problematic PNIE does not cause any issue. Even if there is a special scenario where P'-P for a non-problematic PNIE has more than one root, only one of them corresponds to equilibrium. Therefore, should the iterations converge towards a wrong root, the time step still diverges since the wrong root does not satisfy equilibrium.

It must be noted that for non-differentiable CZM functions with a sharp turning point, the detection process is simple. For instance, if the CZM has a bilinear behavior, the computed interval for the problematic PNIEs at the beginning of iterations shrinks to one point. For a bilinear CZM with convergence difficulty, the starting point of iterations (i.e., the root of previous converged step) cannot go beyond δ_c . Therefore, with a few time step refinements, the starting points of iterations for the problematic PNIEs converge to δ_c . Hence, the problematic PNIEs can easily be detected. It must be noted that a bilinear CZM with a root on its descending portion does not cause convergence issues since the P'-P function is ascending.

4.2. Modification of the problematic PNIEs

Once the problematic PNIEs are detected, the next step is to modify them to a proper starting point of iterations. It must be emphasised that only the starting point of iterations is modified and no displacement is prescribed during the modification process. Fig. 9 (a) illustrates an arbitrary deformation of a cohesive interface with a problematic PNIE. The nodal displacement vectors \mathbf{u}^1 and \mathbf{u}^2 can be extracted directly from the displacement vector of the previous converged step in the global x-y coordinate system. The goal is to calculate \mathbf{u}^1 and \mathbf{u}^2 through vectors \mathbf{c}^1 and \mathbf{c}^2 such that:

- (a) the resulting opening displacement vector of the PNIE (i.e., $\delta' = \mathbf{u}^{1'} \mathbf{u}^{2'}$) is aligned with the opening displacement vector before the modification (i.e., $\delta = \mathbf{u}^1 \mathbf{u}^2$), as it is shown in Fig. 9 (b).
- (b) δ' has a much greater magnitude than δ .

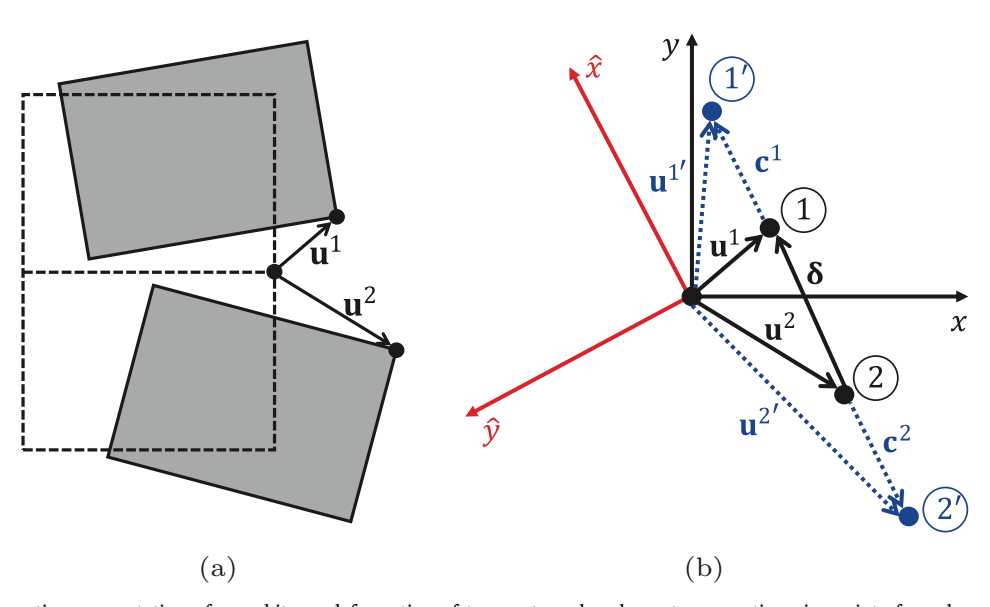


Fig. 9. (a) Schematic representation of an arbitrary deformation of two rectangular elements connecting via an interface element, and (b) the modification applied to the PNIEs' displacement vectors.

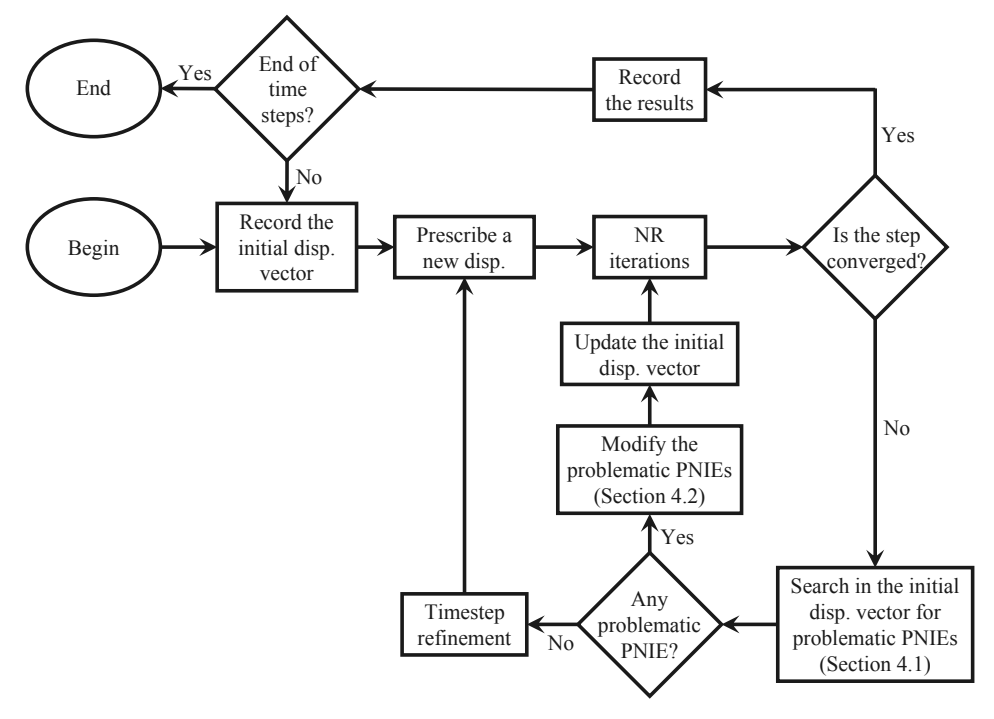


Fig. 10. Implementation algorithm for the proposed NR modification method. The initial disp. vector refers to the starting point of iterations in the NR method

Vectors \mathbf{c}^1 and \mathbf{c}^2 both have arbitrary large magnitudes, and for simplicity, they can be assumed to be equal (i.e., $|\mathbf{c}^1| = |\mathbf{c}^2| = c$). To apply the modification, the vectors \mathbf{u}^1 and \mathbf{u}^2 are first transformed into another orthonormal basis $\hat{x} - \hat{y}$ such that \hat{x} is aligned with δ . The transformation can be performed through a transformation matrix \mathbf{T} as

$$\hat{\mathbf{u}}^1 = \mathbf{T}^{-1}\mathbf{u}^1 = \mathbf{T}^T\mathbf{u}^1$$

$$\hat{\mathbf{u}}^2 = \mathbf{T}^{-1}\mathbf{u}^2 = \mathbf{T}^T\mathbf{u}^2$$
(7)

Now the \hat{x} component of the displacements can be modified as

$$\hat{u}_{\hat{x}}^{1'} = \hat{u}_{\hat{x}}^{1} + c
\hat{u}_{\hat{x}}^{2'} = \hat{u}_{\hat{x}}^{2} - c$$
(8)

After the displacements are modified, the new displacement vectors can be transformed back to the x-y coordinate system as

$$\mathbf{u}^{\mathbf{I}'} = \mathbf{T}\hat{\mathbf{u}}^{1}$$

$$\mathbf{u}^{2'} = \mathbf{T}\hat{\mathbf{u}}^{2}$$
(9)

 \mathbf{u}^{T} and $\mathbf{u}^{2'}$ are the modified values and must be used instead of the old values of \mathbf{u}^{1} and \mathbf{u}^{2} inside the displacement vector at the beginning of the iterations.

A selection guideline for c can be achieved because iterations follow the secant slopes of the material's response where the CZM response contribution in P'-P is zero. Hence, the minimum value for c should be chosen such that $\delta+2c\geqslant\delta_0$, where $\delta+2c$ is the modified debonding of the PNIE and δ_0 is the cohesive debonding corresponding to the cohesive traction $\sigma\to0$. Therefore, c must be selected such that $\delta_0\leqslant\delta+2c\leqslant$ any large positive number.

Fig. 10 presents the algorithm for the implementation of the proposed NR modification method. The algorithm involves detecting the problematic PNIEs and modifying the starting point of iterations. Hence, the method has a simple implementation as it only requires a loop over the displacement vector in the NR method. However, the user implementation of the proposed method within commercial FE codes might not be easily possible due to the users' limited access to the source codes. The non-commercial FE code developers, however, can easily program the proposed algorithm within their frameworks.

5. Verification and application examples

To evaluate the performance of the proposed method, an FE program was developed in Matlab for 2-D analyses, which includes 4-node plane strain and cohesive interface elements. The Gauss quadrature scheme was incorporated in the developed framework for both 4-node and interface elements. For the interfaces, the coupling scenario presented by Eq. (2) was used, with β assumed to be 1.

Five application examples were designed to test the accuracy and performance of the proposed method under different debonding scenarios. The combination of model parameters and dimensions in application examples were designed to induce CZM convergence difficulty. The divergence threshold was set to be 50 iterations. The proposed method was applied automatically when a displacement step diverged. The simulation results using the proposed modification method were compared with Abaqus-implicit [47] and the viscous regularization method.

The viscous regularization method proposed by Gao and Bower [19] was used in the analyses, which introduces the addition of a rate-dependent term to the cohesive law as

$$\sigma_{visc} = \xi \frac{\sigma_c}{\delta_c} \left(\frac{d\delta}{dt} \right) \tag{10}$$

where σ_{visc} is the artificial viscosity that is added to the cohesive function, ξ is the viscosity parameter, and t is the analysis pseudotime. To minimize the effect of the viscous regularization method on the accuracy, ξ was chosen to be the smallest value that prevents the termination of the analysis due to convergence difficulty.

For all the application examples, the material behavior was assumed as elastic under tension and elastic-perfectly-plastic under compression defined by secant stiffness, with a yield strength of 60 MPa. The nonlinear compressive behavior was considered in order to verify that the material's nonlinear behavior under compression does not affect the performance of the proposed method, as discussed in Section 4.

5.1. 2-D bar with a horizontal interface

The first example includes a 1 mm \times 1 mm 2-D bar with a cohesive interface. The displacement is applied to the top boundary, while the vertical displacement of the bottom boundary is restrained. The exponential model presented in Eq. (1) with a σ_c of 60 MPa and a δ_c of 0.02 mm was assumed as the cohesive interface behavior. The Young's modulus (E) and Poisson's ratio (ν) for the material are equal to 1000 MPa and 0, respectively. Three mesh sizes of 1 \times 1, 9 \times 9, and 100 \times 100 were considered to verify that they all yield the same responses. A displacement of 0.2 mm was applied in 100 increments.

Fig. 11 presents the force—displacement responses for the cases with and without the application of the NR modification method. The NR modification was activated only once throughout the analysis, and only three iterations were taken towards convergence of the problematic step. As can be seen in Fig. 11, the analysis could not be completed when the proposed modification was not applied. All different meshing scenarios had the exact same responses as expected. The similar results confirm that the modification does not interrupt the system of equations even though several degrees of freedom were involved.

5.2. Double-cantilever model

The double-cantilever beam is a benchmark example for studying the crack propagation inside materials both experimentally and numerically. Fig. 12 (a) illustrates the configuration of a double-cantilever beam, and Table 1 presents the properties of the model with expected convergence difficulty. The force–displacement response obtained based on the proposed NR modification method is compared with a quasi-static analysis carried out in Abaqus-implicit [47] and the viscous regularization approach to validate the accuracy of the proposed method. It is reminded that the CZMs do not have convergence difficulty in a dynamic analysis. A bilinear CZM was assumed in the analysis, as illustrated in Fig. 12 (b). The bilinear model is available in Abaqus and provides the possibility of a precise comparison. The same mesh size (i.e., 13×50) and element type were used for all three analyses. A displacement of 4 mm was applied in 400 steps. The displacement was applied very slowly at a rate of 0.004 mm/s, the density of the material was set to zero, and a relatively large damping ratio was assumed to minimize dynamic effects in the quasi-static analysis.

Fig. 12 (c) presents the deformed shape of the double-cantilever beam. Fig. 13 (a) demonstrates the force–displacement responses for the dynamic analysis and the static analysis with the NR modification. As it can be seen in this figure, the results are slightly

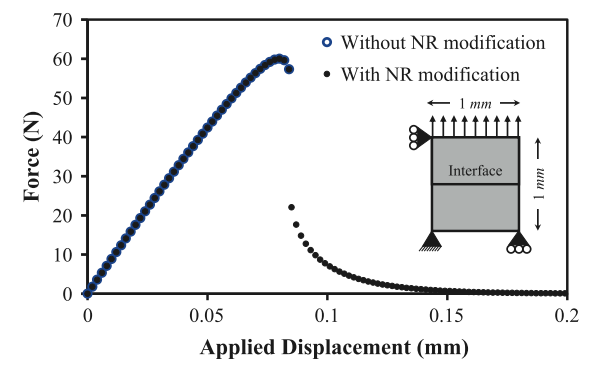


Fig. 11. Force—displacement responses for the 2-D bar with a horizontal interface for the cases with and without the application of the NR modification method.

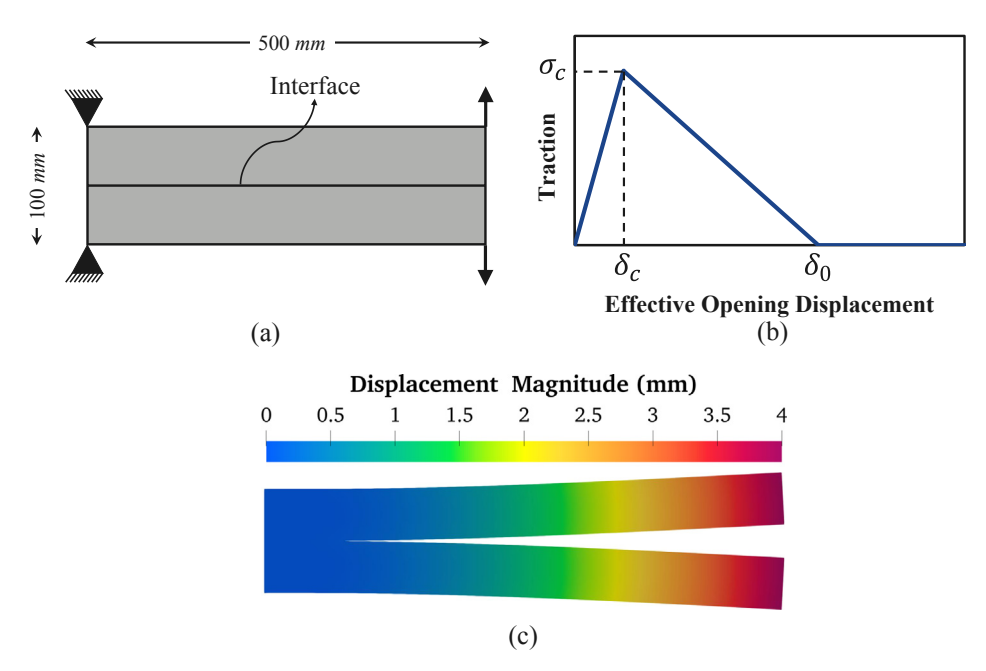


Fig. 12. (a) Boundary conditions, (b) bilinear CZM, and (c) deformed shape for the double-cantilever beam model.

 Table 1

 Material properties for the double-cantilever beam model.

Material Properties				Cohesive Properties (bilinear model)		
E (MPa)	ν	Density (Dynamic)	Rayleigh Damping (Dynamic)	σ_c (MPa)	δ_c (mm)	δ_0 (mm)
20000	0.3	0	0.1	30	0.003	0.033

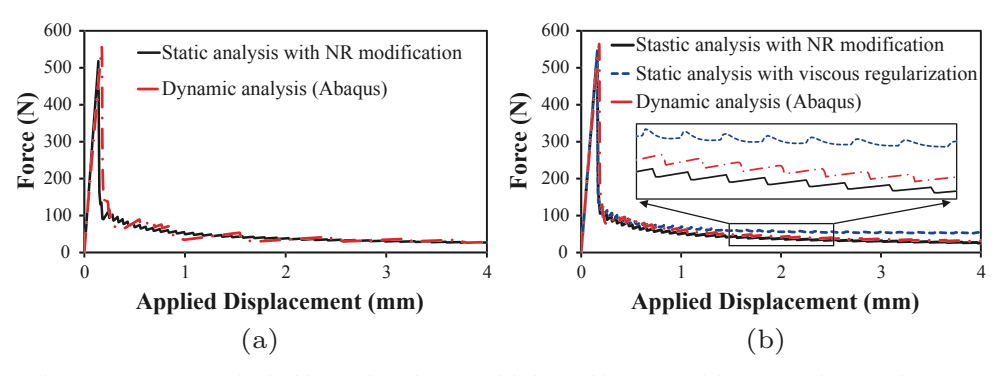


Fig. 13. Force–displacement responses of the double-cantilever beam model obtained by static and dynamic analyses for the cases of (a) $\nu = 0.3$, and (b) $\nu = 0$.

different, because Abaqus does not use the Gauss integration method for first-order elements (i.e., isoparametric 4-node plane stress/strain elements). Abaqus uses a method based on single-point integration, which improves the elements' performance and makes them pass the patch test [47]. One way to minimize the effect of the different integration methods is to set the Poisson's ratio equal to zero. Fig. 13 (b) illustrates the force–displacement responses for the case where the Poisson's ratio is zero. As it can be seen, the results from the static analysis with NR modification matches very well with that of the dynamic analysis, which demonstrates the validity and accuracy of the proposed method. No time step refinement was required throughout the analysis when the proposed method was used. As seen in Fig. 13 (b), the analysis with the viscous regularization method is slightly inaccurate compared to the dynamic analysis, although 113 time step refinements were required.

Fig. 14 (a) illustrates the steps with convergence difficulty that only could converge with the application of the proposed NR

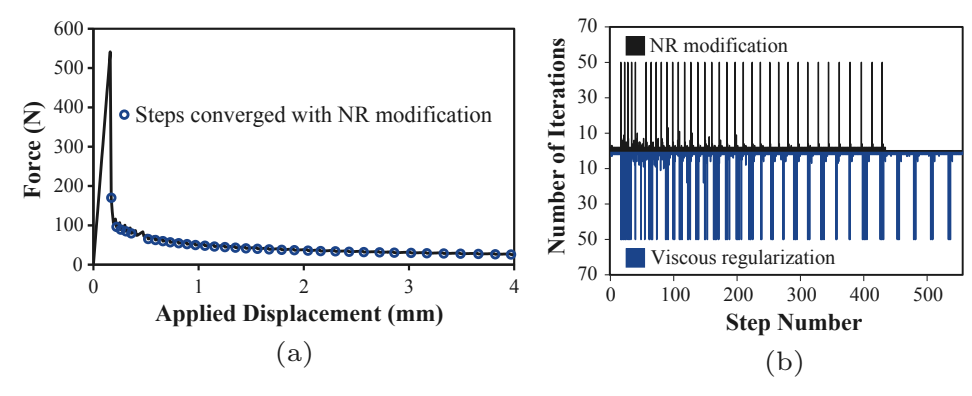


Fig. 14. (a) Force–displacement response of the double-cantilever beam model with $\nu=0$, where the circles demonstrate the steps converged using the modification method, and (b) number of iterations versus time step plot including the diverged steps for the NR modification and viscous regularization methods.

Table 2Material properties for the 2-D bar with two interfaces.

Material Properties		Cohesive Properties (exponential model)				
E (MPa)	ν	σ_{c1} (MPa)	δ _{c1} (mm)	σ _{c2} (MPa)	δ_{c2} (mm)	
2000	0.3	70	0.02	71	0.02	

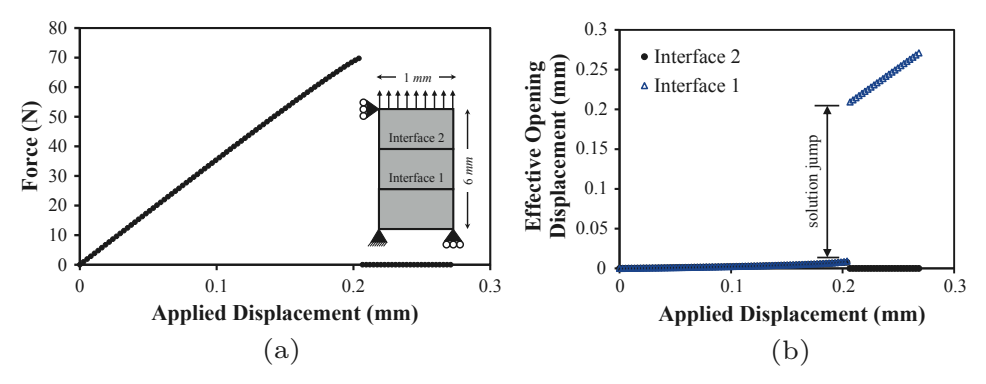


Fig. 15. The 2-D bar with two horizontal interfaces example: (a) force–displacement responses, (b) effective opening displacement versus applied displacement for both interfaces.

modification method for the case of $\nu=0$. A total of 35 steps had convergence difficulty. In the analysis with the viscous regularization method, however, 97 steps had convergence issues and required time step refinements. An average of 6 iterations were taken towards convergence each time the modification method was applied. Fig. 14 (b) compares the number of iterations at each step between the proposed approach and the viscous regularization method. The diverged steps are also included. The figure demonstrates the efficiency of the proposed method over the viscous regularization method. The results presented in Fig. 13 and Fig. 14 confirms that the proposed method is both accurate and computationally efficient.

5.3. 2-D bar with two horizontal interfaces

A 2-D bar with two interfaces was designed to investigate the effect of modifying non-problematic PNIEs. As was described in Section 4.1, there is a possibility that a non-problematic PNIE is detected as problematic, and hence, automatically modified. The designed example here investigates the argued hypothesis that modifying a non-problematic PNIE neither affects the result nor causes any convergence issue.

The example consists of a 1 mm \times 6 mm bar with two interfaces. The top boundary is subjected to vertical displacement while the bottom boundary is vertically restrained. The exponential cohesive model presented in Eq. (1) was assumed for both interfaces. Table 2 presents the model parameters associated with the designed example. A mesh size of 10×60 was considered and displacement of 0.27 mm was applied in 100 increments. To solve this example, the PNIEs detection code was deactivated, and therefore,

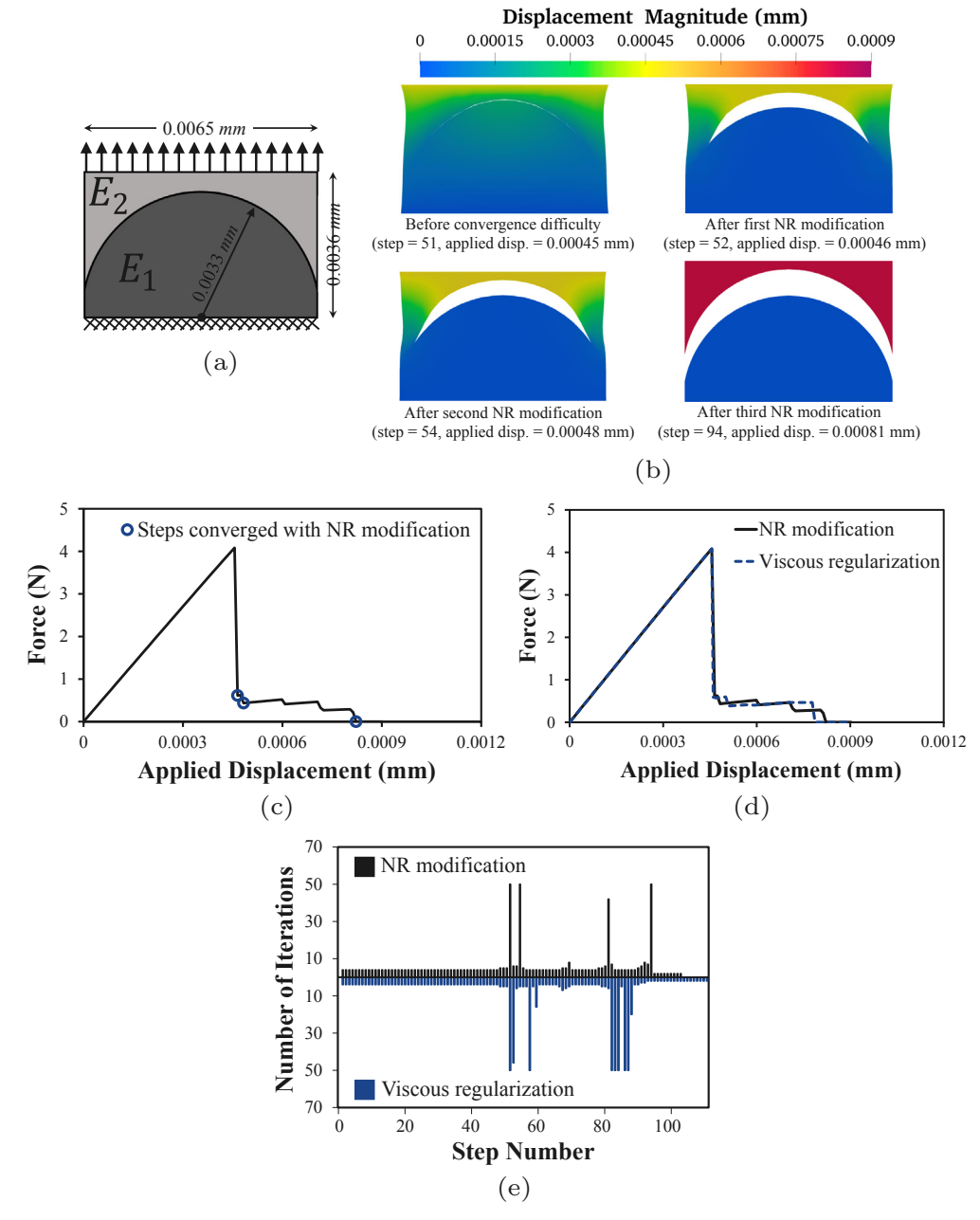


Fig. 16. The 2-D bar with a circular interface example: (a) boundary conditions, (b) deformed shapes at different loading stages when NR modification is used, (c) displacement steps converged with the NR modification method, (d) force—displacement responses for the cases of the NR modification and viscous regularization methods, and (e) analyses' iteration count, comparing the NR modification and viscous regularization methods.

once convergence issue was encountered, the modification was applied to all interface pair nodes.

Fig. 15 (a) illustrates the force–displacement response of the two-interface bar. In this example, the weaker interface with $\sigma_c = 70$ MPa fails, causes convergence difficulty, while the debonding of the other interface recovers. The instantaneous failure and the resulting solution jump is evident in the force–displacement response. Fig. 15 (b) demonstrates the effective opening displacements of the two interfaces versus the applied displacement. It can be seen that there is a solution jump in the weaker interface which fails. Once the weaker interface fails, the other interface unloads, and its debonding recovers. The force–displacement response and iteration counts in the step with convergence issue were compared for the two separate conducted analyses; when the modification was applied to all the interface pair nodes, and when it was only applied to the detected PNIEs. The force–displacement response in both cases were similar. Three iterations were taken towards convergence when the modification was applied to the detected PNIEs (i.e., interface 1). However, when the NR modification was applied to all the interfaces, it only resulted in two additional iterations

Table 3Material properties for the 2-D bar with a circular interface and the fiber-reinforced composite model.

	Material Pro	Cohesive Properties (exponential model)			
E ₁ (MPa)	E ₂ (MPa)	ν_1	ν_2	σ _c (MPa)	δ_c (mm)
		2-D bar with a	circular interface model		
10000	1000	0.3	0.3	1000	0.00005
		Fiber-reinfo	ced composite model		
1000	1000	0.3	0.3	60	0.0001

toward convergence. The presented simple example confirms that modifying a non-problematic PNIE does not affect the convergence of the problem to the accurate root and solutions.

5.4. 2-D bar with a circular interface

The forth example is a 2-D bar composed of two parts with different material properties connected via a circular interface, as illustrated in Fig. 16 (a). The geometry and boundary conditions were designed to force mixed-mode debonding. A displacement of 0.001 mm was applied to the top boundary in 100 increments while the bottom boundary was fixed. The mesh size was adjusted in a way that 20 elements to be along the circle's diameter. The exponential function presented by Eq. (1) was used as the CZM's constitutive behavior. Table 3 presents the properties of the designed model. It must be noted that Abaqus uses a different normal/tangential coupling scenario for the interface than the one used in the developed FE framework in this work (i.e., Eq. (2)). Hence, the result from the static analysis cannot be compared with that of a dynamic analysis using Abaqus. The results are just compared to another static analysis which uses the viscous regularization method to address the convergence issue.

Throughout the analysis, 3 steps had convergence difficulty. Fig. 16 (b) illustrates the deformed shapes of the model corresponding to those problematic steps. As seen in the figure, the interface debonding prior to the first convergence difficulty (i.e., step 51) was small and no interface element failure occurred. The next displacement increment, which required the application of the NR modification method for the convergence, resulted in an instantaneous failure of several interface elements. The last step with convergence difficulty led to the complete separation of the top and bottom parts in the model. Fig. 16 (c) depicts the force–displacement response when the NR modification method was used. The problematic steps which could converge with the application of the proposed method are also marked on the response plot. An average of 5 iterations was taken towards convergence each time the NR modification was applied.

Fig. 16 (d) depicts the force–displacement responses using the proposed NR modification versus the viscous regularization method. The comparison indicates that the results from both studied methods very well match up. The decrease in force after the first NR modification is the same for both methods. However, the post-failure responses are slightly different, which is deemed to be a result of the viscous regularization's negative effect on the accuracy. Fig. 16 (e) shows the number of iterations versus time step for the two analyses with the NR modification and viscous regularization methods. The diverged steps are also included. No time step refinement was required for the convergence of the problematic steps when the proposed method was used. The viscous regularization method, however, required seven time step refinements. This example once again demonstrates that the proposed method is more computationally efficient compared to the viscous regularization method.

5.5. Fiber-reinforced composite model

This example was designed to demonstrate the performance of the proposed method on more complex model geometry. The designed model represents a composite with unidirectional fibers with a diameter of 0.006 mm, subjected to transverse loading. The model geometry and boundary conditions are illustrated in Fig. 17 (a). The top boundary was subjected to a displacement of 0.0028 mm in 50 increments. The mesh size was determined such that 20 elements to be along each fiber's diameter. The fiber/matrix interfaces were modeled using the exponential CZM. Table 3 presents the material properties for the designed model components. The reason for choosing the same E for both fibers and matrix was to force multiple steps with convergence difficulties. The performance of the proposed method was compared to that of the viscous regularization method. A dynamic analysis was not performed since Abaqus uses a different normal/tangential debonding scenario for CZMs.

The analysis had three problematic steps that could converge with the application of the NR modification method. Fig. 17 (b) shows the force–displacement response with the problematic steps marked on it. The deformed shapes of the model corresponding to the modified steps are illustrated in Fig. 17 (c). Prior to the first convergence difficulty (i.e., step 39), the debondings around the fibers were smaller than the specified δ_c , and hence, no interface failure occurred. The convergence of each step with instability was followed by the instantaneous failure of several interface elements. Each instantaneous failure led to debonding recovery in the interfaces that were away from the failure zone. The debonding recovery was also observed in a number of PNIEs that were detected as problematic and modified. Hence, detecting and modifying some non-problematic PNIEs as problematic did not affect the accuracy of the converged solution. The modification did not cause the iterations convergence to a wrong root and did not prevent the

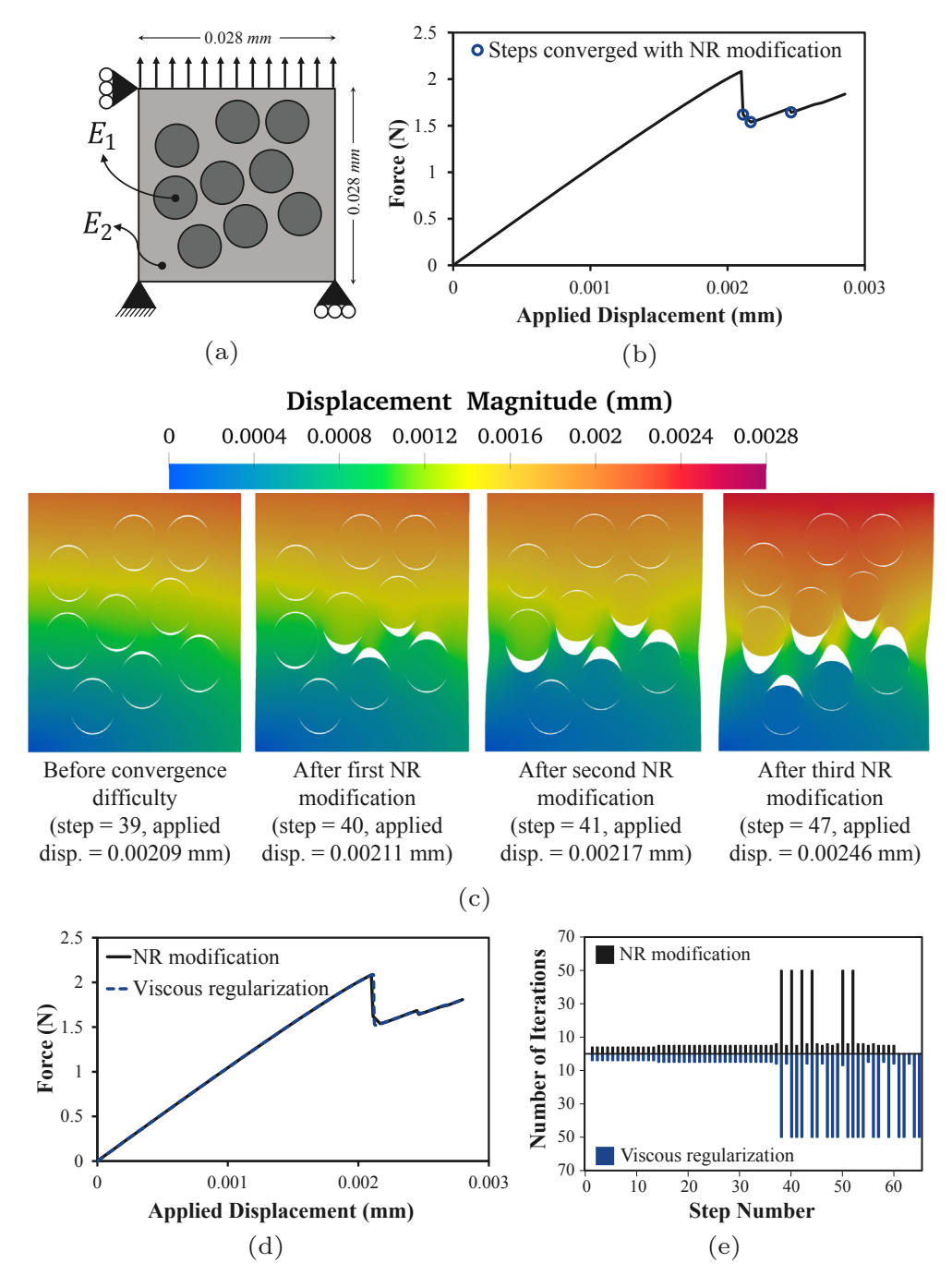


Fig. 17. A composite with circular fibers example: (a) boundary conditions, (b) displacement steps converged with the NR modification method, (c) deformed shapes at different applied displacement when the NR modification is used (scale factor ×2), (d) force–displacement responses using the NR modification and viscous regularization methods, and (e) analyses' iteration count, comparing the NR modification and viscous regularization methods.

unloading of non-problematic interfaces due to the failure of other interfaces.

Fig. 17 (d) illustrates the force–displacement responses obtained using the NR modification and viscous regularization methods. As seen in the figure, the results for both methods are almost identical. Fig. 17 (e) compares the steps iteration count of the proposed approach and the viscous regularization method. The viscous regularization method required 20 time step refinements while for the proposed method, only 3 time step refinements were needed. An average of 5 iterations were taken towards convergence each time the NR modification method was applied. The presented example demonstrates that the proposed method outperforms the viscous regularization method in terms of computational cost.

6. Conclusion

This paper explained the root of the convergence difficulty in CZMs. It was shown that the convergence issue occurs due to numerical instability, which results from the NR iterations entering an infinite cycle. The instability arises in the regions where the material's stiffness is smaller than the CZM's local tangent stiffness. Subsequently, the performance of the two frequently used methods for addressing the convergence difficulty (i.e., viscous regularization method and decrease of global displacement method) was evaluated. It was argued that the methods are either inaccurate, complex, or computationally expensive.

A simple novel method for addressing the convergence difficulty was proposed, which involves a modification to the starting point of iterations in the NR method. It was schematically shown that if the opening displacement of the problematic PNIEs is increased by an arbitrary large value, the convergence issue is addressed. It was explained that the proposed method does not depend on the debonding mode and the material behavior if the secant stiffness defines the materials' constitutive behavior. The detection of the problematic PNIEs was achieved through the introduction of an interval for the starting point of iterations corresponding to problematic PNIEs. The process of detecting and modifying the problematic PNIEs was explained in detail. Five application examples were then presented to evaluate the performance of the proposed method compared to those of the viscous regularization method and dynamic-implicit analysis. The dynamic analysis showcased the precision of the proposed method. The proposed method outperformed the viscous regularization method in terms of both accuracy and computational efficiency.

The proposed method offers fast convergence when applied to CZMs with numerical instabilities. However, for a more quantified evaluation, its performance should be compared with other existing accurate approaches such as the arc-length method. As a final remark, a drawback to the proposed method can be its implementation within existing commercial FE codes. Although the proposed modification method has a straightforward implementation, it deals with the NR algorithm, which is usually out of reach of the users in commercial FE codes.

Declaration of Competing Interest

The authors declare no potential conflict of interests.

Acknowledgments

The authors like to acknowledge the support for this paper by the Virginia Tech Start-up funding and National Science Foundation award (Grant No. 1853893).

Appendix A. Supplementary material

Supplementary data associated with this article can be found, in the online version, at https://doi.org/10.1016/j.engfracmech. 2020.107046.

References

- [1] Roe K, Siegmund T. An irreversible cohesive zone model for interface fatigue crack growth simulation. Eng Fract Mech 2003;70(2):209-32.
- [2] Aymerich F, Dore F, Priolo P. Prediction of impact-induced delamination in cross-ply composite laminates using cohesive interface elements. Compos Sci Technol 2008;68(12):2383–90.
- [3] Carloni C, Subramaniam KV, Savoia M, Mazzotti C. Experimental determination of FRP-concrete cohesive interface properties under fatigue loading. Compos Struct 2012;94(4):1288-96.
- [4] Herráez M, Mora D, Naya F, Lopes CS, González C, LLorca J. Transverse cracking of cross-ply laminates: a computational micromechanics perspective. Compos Sci Technol 2015;110:196–204.
- [5] Turon A, González E, Sarrado C, Guillamet G, Maimí P. Accurate simulation of delamination under mixed-mode loading using a cohesive model with a mode-dependent penalty stiffness. Compos Struct 2018:184:506–11.
- [6] Shakiba M, Brandyberry DR, Zacek S, Geubelle PH. Transverse failure of carbon fiber composites: analytical sensitivity to the distribution of fiber/matrix interface properties. Int J Numer Meth Eng 2019;120(5):650–65. https://doi.org/10.1002/nme.6151.
- [7] Zamani A, Gracie R, Reza Eslami M. Cohesive and non-cohesive fracture by higher-order enrichment of xfem. Int J Numer Meth Eng 2012;90(4):452-83.
- [8] Wang Y, Waisman H. Progressive delamination analysis of composite materials using xfem and a discrete damage zone model. Comput Mech 2015;55(1):1–26.
- [9] Wang Y, Waisman H. From diffuse damage to sharp cohesive cracks: A coupled xfem framework for failure analysis of quasi-brittle materials. Comput Methods Appl Mech Eng 2016;299:57–89.
- [10] Chaboche J, Feyel F, Monerie Y. Interface debonding models: a viscous regularization with a limited rate dependency. Int J Solids Struct 2001;38(18):3127-60.
- [11] Hamitouche L, Tarfaoui M, Vautrin A. An interface debonding law subject to viscous regularization for avoiding instability: application to the delamination problems. Eng Fract Mech 2008;75(10):3084–100.
- [12] Dimitri R, Trullo M, Zavarise G, De Lorenzis L. A consistency assessment of coupled cohesive zone models for mixed-mode debonding problems. Frattura ed Integrità Strutturale 2014;8(29):266–83.
- [13] Yu H, Olsen JS, Olden V, Alvaro A, He J, Zhang Z. Viscous regularization for cohesive zone modeling under constant displacement: an application to hydrogen embrittlement simulation. Eng Fract Mech 2016;166:23–42.
- [14] Volokh KY. Comparison between cohesive zone models. Commun Numer Methods Eng 2004;20(11):845-56.
- [15] Jiang H. Cohesive zone model for carbon nanotube adhesive simulation and fracture/fatigue crack growth, Ph.D. thesis. University of Akron; 2010.
- [16] Needleman A. Some issues in cohesive surface modeling. Procedia IUTAM 2014;10:221–46.
- [17] Zhu W, Yang L, Guo J, Zhou Y, Lu C. Determination of interfacial adhesion energies of thermal barrier coatings by compression test combined with a cohesive zone finite element model. Int J Plast 2015;64:76–87.
- [18] Simonovski I, Cizelj L. Cohesive zone modeling of intergranular cracking in polycrystalline aggregates. Nucl Eng Des 2015;283:139-47.
- Gao Y, Bower A. A simple technique for avoiding convergence problems in finite element simulations of crack nucleation and growth on cohesive interfaces.

- Modell Simul Mater Sci Eng 2004;12(3):453.
- [20] Gu Y, Jung J, Yang Q, Chen W. An inertia-based stabilizing method for quasi-static simulation of unstable crack initiation and propagation. J Appl Mech 2015;82(10):101010.
- [21] Hilber HM, Hughes TJ, Taylor RL. Improved numerical dissipation for time integration algorithms in structural dynamics. Earthq Eng Struct Dyn 1977;5(3):283–92
- [22] Hilber HM, Hughes TJ. Collocation, dissipation and [overshoot] for time integration schemes in structural dynamics. Earthq Eng Struct Dyn 1978;6(1):99-117.
- [23] Michel B, Helfer T, Ramière I, Esnoul C. A new numerical methodology for simulation of unstable crack growth in time independent brittle materials. Eng Fract Mech 2018;188:126–50.
- [24] Riks E. An incremental approach to the solution of snapping and buckling problems. Int J Solids Struct 1979;15(7):529-51.
- [25] Needleman A. An analysis of tensile decohesion along an interface. J Mech Phys Solids 1990;38(3):289-324.
- [26] Ortiz M, Pandolfi A. Finite-deformation irreversible cohesive elements for three-dimensional crack-propagation analysis. Int J Numer Meth Eng 1999:44(9):1267–82.
- [27] Chandra N, Li H, Shet C, Ghonem H. Some issues in the application of cohesive zone models for metal–ceramic interfaces. Int J Solids Struct 2002;39(10):2827–55.
- [28] Hillerborg A, Modéer M, Petersson P-E. Analysis of crack formation and crack growth in concrete by means of fracture mechanics and finite elements. Cem Concr Res 1976;6(6):773–81.
- [29] Mi Y, Crisfield M, Davies G, Hellweg H. Progressive delamination using interface elements. J Compos Mater 1998;32(14):1246-72.
- [30] Alfano G, Crisfield M. Finite element interface models for the delamination analysis of laminated composites: mechanical and computational issues. Int J Numer Meth Eng 2001;50(7):1701–36.
- [31] Tvergaard V, Hutchinson JW. The relation between crack growth resistance and fracture process parameters in elastic-plastic solids. J Mech Phys Solids 1992;40(6):1377–97.
- [32] Tvergaard V, Hutchinson JW. The influence of plasticity on mixed mode interface toughness. J Mech Phys Solids 1993;41(6):1119-35.
- [33] Allix O, Ladeveze P, Corigliano A. Damage analysis of interlaminar fracture specimens. Compos Struct 1995;31(1):61-74.
- [34] Allix O, Corigliano A. Modeling and simulation of crack propagation in mixed-modes interlaminar fracture specimens. Int J Fract 1996;77(2):111-40.
- [35] Alfano G. On the influence of the shape of the interface law on the application of cohesive-zone models. Compos Sci Technol 2006;66(6):723-30.
- [36] Tvergaard V. Effect of fibre debonding in a whisker-reinforced metal. Mater Sci Eng: A 1990;125(2):203-13.
- [37] Geubelle PH, Baylor JS. Impact-induced delamination of composites: a 2D simulation. Compos Part B: Eng 1998;29(5):589-602.
- [38] Wang Y, Waisman H. An arc-length method for controlled cohesive crack propagation using high-order XFEM and Irwin's crack closure integral. Eng Fract Mech 2018;199:235–56.
- [39] Liu P, Gu Z, Hu Z. Revisiting the numerical convergence of cohesive-zone models in simulating the delamination of composite adhesive joints by using the finite-element analysis. Mech Compos Mater 2016;52(5):651–64.
- [40] Truster TJ, Eriten M, Polycarpou AA, Bergman LA, Masud A. Stabilized interface methods for mechanical joints: Physics-based models and variationally consistent embedding. Int J Solids Struct 2013;50(14–15):2132–50.
- [41] Truster TJ, Masud A. A discontinuous/continuous galerkin method for modeling of interphase damage in fibrous composite systems. Comput Mech 2013;52(3):499–514.
- [42] Truster TJ, Masud A. Discontinuous galerkin method for frictional interface dynamics. J Eng Mech 2016;142(11):04016084.
- [43] Chen P, Truster TJ, Masud A. Interfacial stabilization at finite strains for weak and strong discontinuities in multi-constituent materials. Comput Methods Appl Mech Eng 2018;328:717–51.
- [44] Tvergaard V. Micromechanical modelling of fibre debonding in a metal reinforced by short fibres. Inelastic deformation of composite materials. Springer; 1991. p. 99–111.
- [45] Peerlings RH, de Borst R, Brekelmans WM, De Vree J. Gradient enhanced damage for quasi-brittle materials. Int J Numer Meth Eng 1996;39(19):3391-403.
- [46] de Borst R, Remmers JJ. Computational modelling of delamination. Compos Sci Technol 2006;66(6):713–22.
- [47] Hibbitt H, Karlsson B, Sorensen P. Abaqus analysis user's manual version 6.10, Dassault Systèmes Simulia Corp.: Providence, RI, USA; 2011.